coatings

MDPI

Article

Mechanical Properties, Biocompatibility and Antibacterial Behaviors of $TaO_{0.2}N_{0.8}$ and $TaO_{0.2}N_{0.8}$-Ag Nanocomposite Thin Coatings

Jang-Hsing Hsieh [1,2,3,4,*], Chuan Li [2,*], Weite Wu [4], Yi-Hwa Lai [3], Shu-Chuan Liao [5], Chih-Chien Hu [6,7] and Yu-Han Chang [6,7]

1 Department of chemical and Materials Engineering, Center for Green Technology, Chang Gung University, Taoyuan 33302, Taiwan
2 Department of Biomedical Engineering, National Yang Ming Chiao Tung University, Taipei 300093, Taiwan
3 Center for Plasma and Thin Coating Technologies, Ming Chi University of Technology, New Taipei 24301, Taiwan
4 Metals Research and Development Center, National Chung Hsing University, Taichung 402, Taiwan
5 Bachelor Program for Design and Materials for Medical Equipment and Devices, Da Yeh University, Chunghwa 515006, Taiwan
6 College of Medicine, Chang-Gung University, Taoyuan 33302, Taiwan
7 Bone and Joint Research Center, Chang Gung Memorial Hospital, Kweishan, Taoyuan 33305, Taiwan
* Correspondence: jhhsieh@mail.mcut.edu.tw (J.-H.H.); cli10@nycu.edu.tw (C.L.)

Abstract: $TaO_{x=0.2}N_{y=0.8}$ was reported previously to have the highest modulus (E), hardness (H), and H to E ratio attributed to the embedment of substituting oxygen atoms in the TaN crystal structure, among some TaOxNy coatings studied. In the present study, $TaO_{0.2}N_{0.8}$-Ag nanocomposite coatings were fabricated by reactive multi-target sputtering with O/N ratio adjusted to the expected value. The various Ag contents were doped to induce antibacterial behaviors. After deposition and annealing with rapid thermal process (RTP) at 400 °C for 4 min, the coatings' mechanical and structural properties were studied. After these examinations, the samples were then studied for their cell attachment, cell viability, and biocompatibility with 3-T-3 cells, as well as for their antibacterial behaviors against Escherichia coli. It appeared that hardness and crack resistance could be improved further with suitable amount of Ag doped to the coatings, followed by rapid thermal annealing treatment. The coating with 1.5 at. % Ag had the highest hardness and good H/E ratio. It was also found that the antibacterial efficiency of $TaO_{0.2}N_{0.8}$-Ag coatings could be much improved, comparing with that of $TaO_{0.2}N_{0.8}$ coatings. The antibacterial efficiency increased with the increased Ag contents. There was no negative effect of Ag on the biocompatibility of $TaO_{0.2}N_{0.8}$-Ag. Through the cell attachment and viability testing using MTT(3-(4,5-Dimethylthiazol-2-yl)-2,5-diphenyltetrazolium bromide) assay, it can be summarized that surface roughness could be the dominating factor for cell viability and attachment, which means the improvement of biocompatibility. Accordingly, the samples with 1.5 at. % and 11.0 at. % Ag show the best biocompatibility. The variation of surface roughness was affected by the incorporation of Ag and oxygen atoms after rapid thermal annealing.

Keywords: tantalum oxynitride; nanocomposite thin coatings; Ag; antibacterial behavior; biocompatibility; surface roughness

check for updates

Citation: Hsieh, J.-H.; Li, C.; Wu, W.; Lai, Y.-H.; Liao, S.-C.; Hu, C.-C.; Chang, Y.-H. Mechanical Properties, Biocompatibility and Antibacterial Behaviors of $TaO_{0.2}N_{0.8}$ and $TaO_{0.2}N_{0.8}$-Ag Nanocomposite Thin Coatings. *Coatings* **2023**, *13*, 88. https://doi.org/10.3390/coatings13010088

Academic Editor: Alessandro Latini

Received: 1 November 2022
Revised: 4 December 2022
Accepted: 27 December 2022
Published: 3 January 2023

Copyright: © 2023 by the authors. Licensee MDPI, Basel, Switzerland. This article is an open access article distributed under the terms and conditions of the Creative Commons Attribution (CC BY) license (https://creativecommons.org/licenses/by/4.0/).

1. Introduction

It has been reported that coatings embedded with Ag nano particles (Ag NPs) could enhance the bioactivity and osseointegration of surgical implants in the field of orthopedics and orthodontics [1]. Ag NPs formed on oxide or nitride coatings could critically reduce the infection possibility of surgical implants by providing coatings with resistance to bacterial contamination and colonization. In addition, it is reported that these coatings may be beneficial on osteogenic activity [2,3] According to some previous reports, Ag ions could

illuminate at least 16 different types of bacteria [4,5]. Silver ions can cause the death of bacteria by impairing the cell walls by oxidation, stop protein production and interfere those signals for replication. In addition, the energy-related surviving processes may be obstructed [4,5]. The Ag-containing nanocomposite coatings can act synergistically, as the Ag NPs provide their antimicrobial effects, while the coating body provides protection against mechanical damage and corrosion attack, and also maintain biocompatibility.

Recently, tantalum-based thin ceramic coatings embedded with soft metals (i.e., TaN-Ag, TaN-Cu, as well as the combination) were fabricated by a sequentially dual process starting with reactive multi-target sputtering followed by annealing with rapid thermal process (RTP) at temperatures around 400 °C [6,7]. Tantalum-based alloys and coatings are well known for their excellent bio-related behaviors which include biocompatibility and corrosion resistance. Hence, it can be said that tantalum nitride will be a good choice for bio-related applications [8]. Ag, as an additive element, was shown not miscible with TaN at all. Hence, theoretically, making TaN-Ag nanocomposite coating is quite possible [7,9]. In this case, Ag NPs can be either formed on the surface or segregated in the TaN coatings.

Furthermore, oxynitrides of transition metals was reported to have tunable mechanical and biological behaviors when the oxygen to nitrogen concentration ratio was changed [10–13]. Theoretically, even with a little change on the ratio of oxygen in the nitride structure, the oxynitride's chemical and physical properties will definitely change too. Normally, nitrogen is less electronegative, the bonds between metal and nitrogen atoms are definitely more covalent than the bonds between and oxygen atoms [14–16]. Without any doubt, the variation of O/N ratio in oxynitride materials would cause the change of some characteristic properties. In their study of TaOxNy, Banakh et al. [17] reported the surface roughness of TaOxNy coatings could reach its highest value, with just small addition of oxygen atoms into the coatings. When biocompatibility is concerned, it is generally known that roughened devices' surface in nanoscale should be advantageous for cell attachment and biocompatibility. Unfortunately, there have been few studies focusing on the bio-related behaviors of oxynitride, especially with the segregation of Ag NPs. The enhancement of nano-roughness as well as the improved mechanical properties should be advantageous in some of the bio-related applications involving oxynitride coatings. Regarding the enhanced mechanical properties, Banakh et. al. [17] reported that proper oxygen atoms added into nitride layers may form dense Zone T structure, resulting in enhanced hardness and increased roughness. Here, in a short summary, with proper addition of oxygen atoms to nitride structure, the oxy-nitride coatings would have various morphologies as well as physical and chemical properties. These improved properties would eventually result in many beneficial effects on the behaviors of the coatings, including biological applications.

As reported previously [18], TaOxNy films could be fabricated by reactive multi-target sputtering with the variation oxygen flowrates. With increasing oxygen concentrations in the film, the structure could transform from cubic TaN phase to TaON phase, finally to Ta-oxide phase with amorphous structure. Another study by our group shows that the oxynitride coatings prepared with 0.3 sccm oxygen flow rate would induce a film with the highest modulus (E), hardness (H), as well as the highest ratio of H/E [19]. This was thought to be attributed to that oxygen atoms substituted some nitrogen atoms, while the crystal structure remained unchanged. This would result in the generation of great strain energy, which would eventually improve the mechanical properties. When the coatings deposited with high oxygen contents, poor biocompatibility was observed, which was caused by their low surface energy and low surface roughness. Furthermore, it is believed that besides other important properties, Ag atoms can be embedded into TaOxNy coatings to improve antibacterial behaviors of the oxynitride. So far, there is no systematical study on the influence of Ag concentrations on the antibacterial properties, and biocompatibility of the mechanically optimized oxy-nitride coatings. In the present study, various amount of Ag was doped into $TaO_{0.2}N_{0.8}$ (oxygen flow rate = 0.3 sccm) coatings in order to understand further the involvement of Ag on the mechanically optimized TaOxNy coatings. One of

the important goals in this study is to examine the possible cytotoxicity of Ag dopants embedded in/on the coatings.

2. Materials and Methods

2.1. Deposition

$TaO_{0.2}N_{0.8}$ and $TaO_{0.2}N_{0.8}$-Ag coatings were fabricated using reactive multi-target sputtering with, Ag and Ta. The coatings were prepared on Si (001) substrates without any extra heating. The attached round targets all had 50 mm in diameter. They were 30° off the normal line of substrate surface. The target-to-substrate distance was 100 mm. during deposition, the deposition system was vacuumed until 7×10^{-4} Pa was reached. The chamber was then introduced with Ar gas up to 0.65 Pa. The substrates used in the experiment were cleaned in ultrasonic cleaner with acetone, isopropanol, and deionized water, each for 5 min., followed by a drying process with a nitrogen jet. Before starting the process, all the targets were plasma cleaned in Ar atmosphere for 10 min, during which the target shutter was closed. In the step of target cleaning, the substrates were also cleaned with Ar plasma. In substrate cleaning, the 100 W (RF) bias was applied. For deposition, the Ta target power was fixed at 190 W. In addition, a 40 W(RF) bias was applied onto the substrate holder. The Ag target power was adjusted in order to provide 0 at. %, 1.5 at. %, 7 at. % and 11 at. % Ag in the $TaO_{0.2}N_{0.8}$-Ag coatings. During the process of coating deposition, the flow of nitrogen was fixed at 4.5 sccm, while the flow of oxygen was kept constant at 0.3 sccm, as explained previously. Under these deposition parameters, the hardness of $TaO_{0.2}N_{0.8}$ coating reached 24 GPa. (Without oxygen, the hardness of TaN coating was around 20 GPa.). The coating thickness was around 1 μm. A surface profiler (Kosaka Surfcoder, Tokyo, Japan) was applied to measure the thickness of coatings. In between the substrate and oxynitride layer, thin Ta/TaN layers (50/100 nm) were first deposited in order to enhance the adhesion. Some selected coatings were annealed for 4 min at 400 °C in a rapid thermal process (RTP) system (SJ, ARTS-150,JIPLEC, Hsinchu, Taiwan). The RTP was carried out in argon atmosphere. All the annealing processes had a ramping rate controlled at 100 °C/s. The annealing temperatures was selected according to a previous study on TaN-Ag. In their study, a DSC (Differential Scanning Calorimeter, Perkin Elmer, Akron, OH, USA) was used to determine the segregation temperature of Ag NPs. [20]. According to the results, it showed that Ag atoms should begin to out-diffuse at 250 °C. The diffusion rate reached the peak at 325 °C, and finish before 400 °C. Therefore, the RTA temperature was set at 400 °C in this study in order to assure that Ag NPs could emerge out. At the same time, the temperature would not be too high to cause unnecessary diffusions or reactions.

2.2. Thin Coating Characterization

The nano mechanical testing (i.e., modulus and hardness) of the coatings were carried out by applying a nano-indenter (Hysitron triboindenter TI-900, Minneapolis, MN, USA). In this system, a Berkovich tip was adopted. Before the testing, the calibration of tip area function was performed following a procedure which was summarized by Oliver and Pharr [21]. According to a previous report [22], It is required that the indentation depth should be set at one-tenth or less of the layer thickness to avoid the influence incurred by the substrate. Nanoindentation technique is now well accepted as a robust method for the determination of mechanical properties of thin layers, because of low load, small contact area, and reliable mathematic model. Which cannot be carried out by traditional testing approaches. The conventional testing approaches are basically not feasible. Traditional testing approaches, including tensile testing or dynamic mechanical analysis (DMA), normally can only acquire the results on the average scale. There is no way to obtain the variability on an area with small scale. The sample size reduction allows the nanoindentation technique to be used onto a relatively small surface. However, the limitation of nanoindentation technique is that the calculation of elastic modulus which is calculated from the unloading part of the testing curve. The calculation goes through a

process that requires the material to be linear and isotropic. In present work, we applied the displacement control mode, with the loading rate set at 1 nm/s. Eight measurements were performed on each sample. The modulus and hardness were obtained according to Oliver and Pharr approach [21]. For the coating morphology investigation, it was carried out using field-emission scanning electron microscopy (FESEM, 15 kV, JEOL 6700F, Tokyo, Japan). The structural and phase analyses of the coatings were examined by X-ray diffractometry (XRD, Philips PW 1830, Caerphilly, UK). Through this characterization, the existence of Ag phases could be examined. The X-ray diffractometer applied monochromatic Cu Kα beam (λ = 0.1541 nm). During the tests, the system scanned through 25°-2θ to 65°-2θ. The step size was set at 0.04°. The measurement time per step was set at 1.60 s. The surface profile as well as nano-roughness was examined by applying atomic force microscopy (AFM, Digital Instruments-Dimension 3100, Veeco, New York, NY, USA). The AFM was applied to obtain the information of Ra and Rmax. Both were the quantification of surface roughness. Ra is well accepted to be the average of the absolute distance value away from the average profile line. It is the most widely used roughness index up to date. Rmax was also measured here as the second index to act as cross reference for roughness. Rmax is the difference from the position of the highest peak to the position of the lowest valley of the profile. For the elemental analysis, WDS (Wavelength Dispersive Spectrometer, JSM-7610F, Akishima, Kyoto, Japan) was adopted. The percentage error is about 5%. During the experiment, the target power has to be adjusted from time to time in order to get right atomic percentage.

For the biocompatibility testing, 3T3 mouse embryo fibroblast cells were used. During the test, three same coating samples were placed in a 24 well plate holder. Each testing well contained cell suspension of 2×10^4 cells. The temperature was controlled at 37 °C. The biocompatibility was evaluated based on the observation of the fibroblast's cell attachment appeared on the sample surface. Here, we used optical microscopy to take photo and observe, at the end of 1, 3, 5 and 7 days. For checking the cell viability, the well-known MTT assay testing was also performed. The MTT testing [3-(4,5-dimethylthiazol-2-yl)-2,5-dipenyl tetrazolium bromide, Sigma] was carried out following the standard operation procedures. At the end, the cells were then lysed using dimethyl sulfoxide (DMSO) for dissolving the condensed crystals. The dissolved solution was examined using an ELISA plate reader. The absorptive wavelength of 570 nm was aimed and examined. This absorption intensity would stand for the cell viability.

For the antibacterial testing, the testing samples with 2 cm × 2 cm dimension were immersed in the bacterial suspension, containing *Escherichia coli* (*E. coli*). The bacteria concentration was 1×10^8 CFU. Next, the solution was incubated at 37 °C. Following this procedure, the antibacterial behavior was examined and compared using Antibacterial Efficiency Index (E). The index was determined using the following equation:

$$E\ (\%) = [(A - B)/A] \times 100\% \quad (1)$$

where A = number of viable bacteria with the uncoated sample; B = number of viable bacteria with the coated sample. Three samples were tested each condition, and then the averaged antibacterial efficiency was evaluated.

3. Results and Discussion

3.1. Structural Analysis

The X-ray diffraction patterns of $TaO_{0.2}N_{0.8}$-Ag coatings, before and after being annealed at 400 °C for 4 min, are presented in Figure 1. It can be observed that these coatings only show the diffraction peaks of TaN structure (ICDD card 04-019-2403). Apparently, oxygen atoms only substitute for some nitrogen atoms under the selected coating parameters. After rapid thermal annealing, Ag (111) peak intensity becomes more obvious and sharper with the increase of Ag contents, which means Ag particles emerging out and becoming larger with the increase of Ag contents. It is also observed the coatings deposited with 11 at. % Ag tend to have sharper diffraction peak after annealing. By measuring the FWHM (Full Width Half Maximum) of TaN (111) peaks, the normalized FWHM, based on TaN (111)

peak of the annealed $TaO_{0.2}N_{0.8}$-Ag with 1.5 at. % Ag, could be estimated. The results are shown in Table 1. According to the results, the sample with 11 at. % Ag shows the largest change on normalized FWHM. It is believed that the additional Ag in $TaO_{0.2}N_{0.8}$ matrix would possibly induce the crystallization of $TaO_{0.2}N_{0.8}$ through the creation of interface (heterogeneous nucleation) since Ta and Ag are completely immiscible [23]. Regarding the detailed mechanism, further study is required.

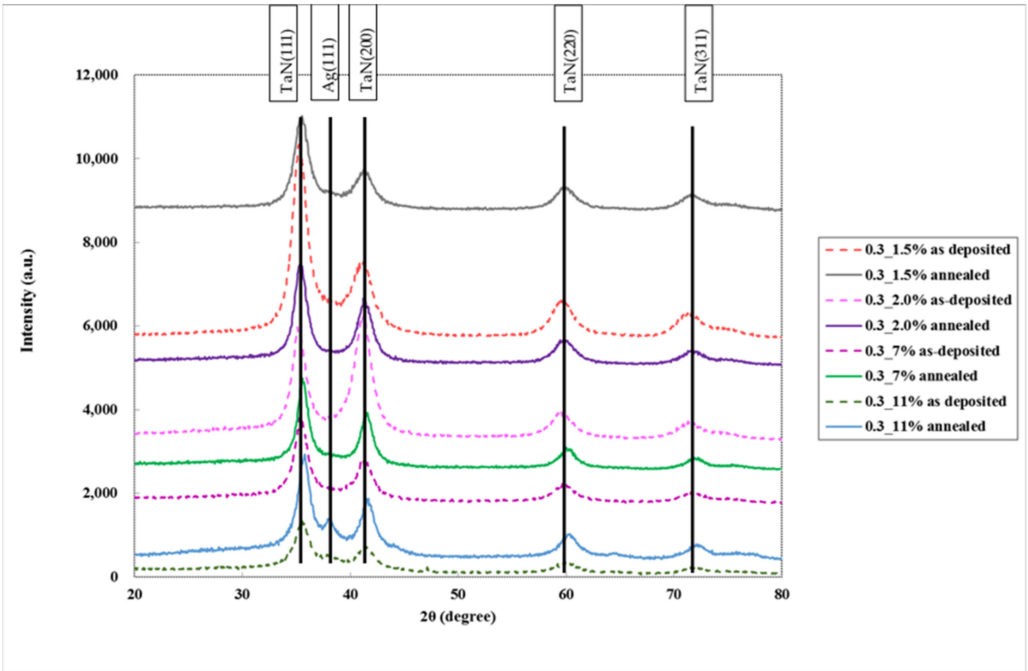


Figure 1. X-ray diffraction patterns for $TaO_{0.2}N_{0.8}$ and $TaO_{0.2}N_{0.8}$-Ag coatings with and without annealing. (Note: The first number of the sample designation stands for oxygen gas flow rate, the 2nd number stands for Ag atomic percentage in the coatings.).

Table 1. Normalized FWHM of TaN (111) peaks based on the sample of annealed $TaO_{0.2}N_{0.8}$-Ag with 1.5 at. % Ag.

FWHM (Degree-2θ)	$TaO_{0.2}N_{0.8}$-Ag-1.5 at. % Ag	$TaO_{0.2}N_{0.8}$-Ag-at. 2% Ag	$TaO_{0.2}N_{0.8}$-Ag-7 at. % Ag	$TaO_{0.2}N_{0.8}$-Ag-11 at. % Ag
As deposited	3.8	3.9	4.75	8.0
Annealed	2.2	3.2	3.75	3.8

Figure 2 shows the cross-sectional SEM micrographs of $TaO_{0.2}N_{0.8}$ and $TaO_{0.2}N_{0.8}$ coatings with and without annealing. The surface views of the annealed samples are presented in Figure 3. The emerged particles can be observed on coating's surface. In this Figure, the Ag element mapping by EDS on the sample with 11 at. % Ag is shown in Figure 3d.

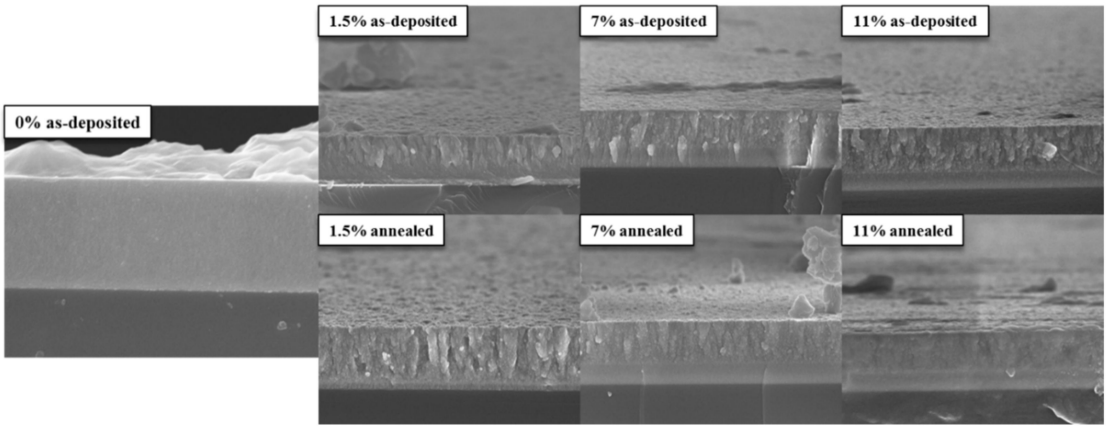


Figure 2. Cross-sectional SEM micrographs of $TaO_{0.2}N_{0.8}$ and $TaO_{0.2}N_{0.8}$-Ag coatings with and without annealing. (Note: The numbers in sample designation standard for the atomic percentage of Ag in the coating).

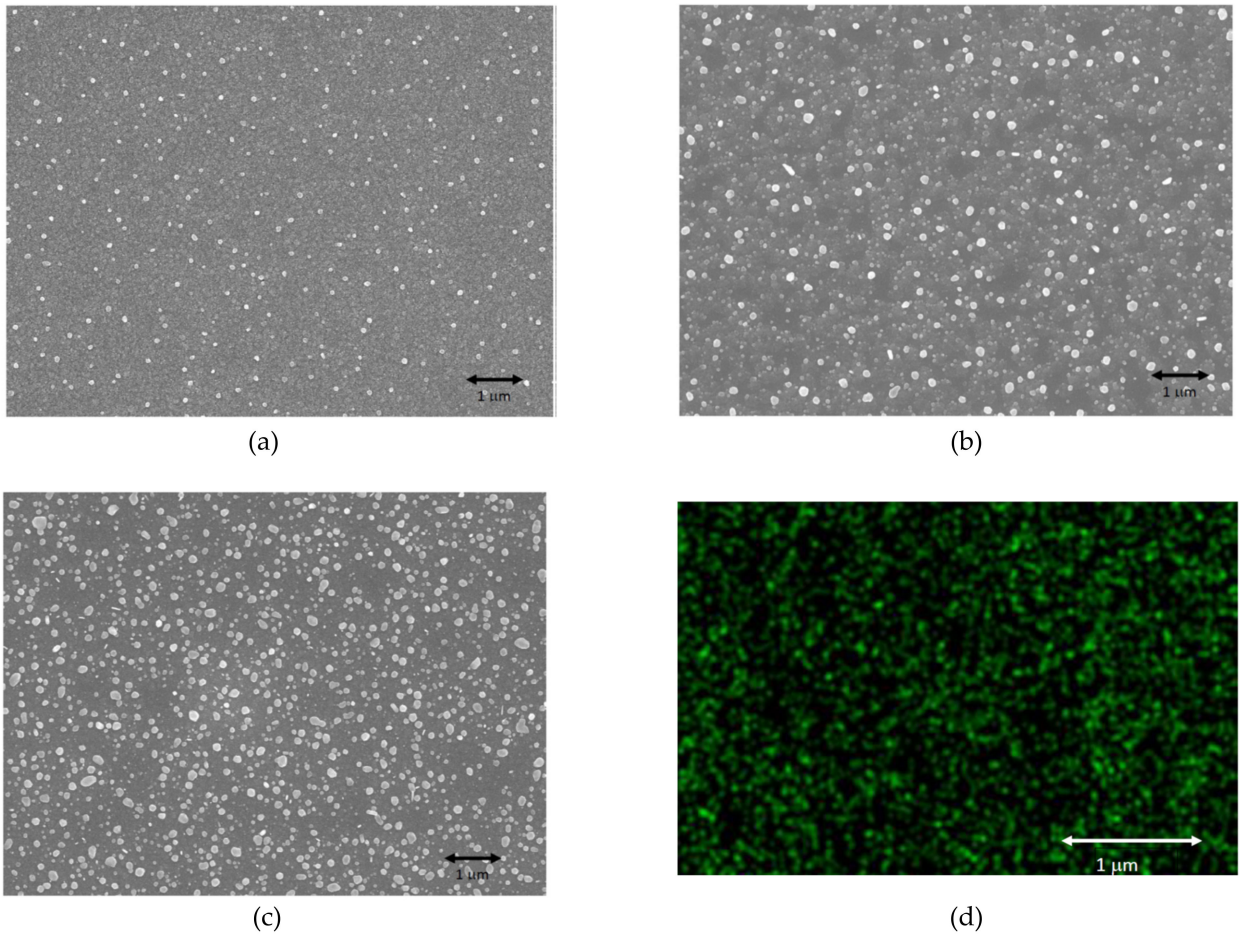
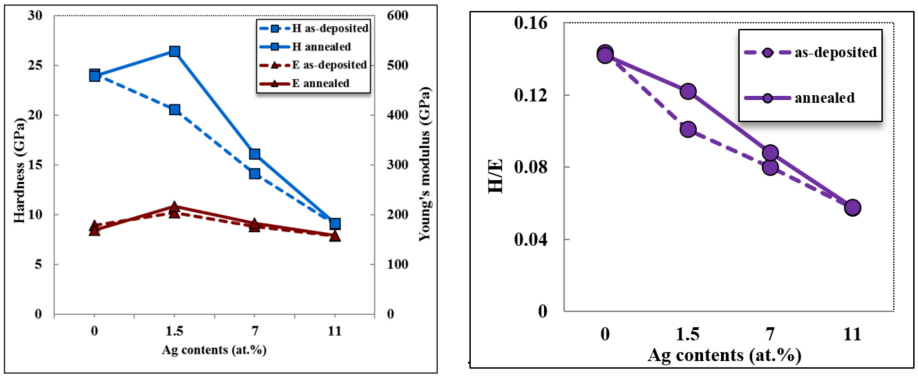


Figure 3. The surface views of the annealed samples: (**a**) 1.5 at % Ag; (**b**) 7.0 at. % Ag; (**c**) 11 at % Ag; (**d**) Ag mapping of (**c**).

3.2. Mechanical Properties

Figure 4a shows hardness and modulus values of $TaO_{0.2}N_{0.8}$ and $TaO_{0.2}N_{0.8}$ coatings with and without annealing. It is observed that the hardness values of the as-deposited samples decrease with the increase of Ag contents, while the modulus increases then decreases. However, after annealing, the hardness and modulus of the coatings reach the maximum point with Ag contents at 1.5 at. %. It is known that over doping with soft metal

in hard coating may disrupt the growth of dense columnar structure, which, in turn, would decrease the hardness. On the other hand, porosity and structure, in general, could also affect the hardness of sputtered coatings, by examining the cross-sectional SEM images as shown in Figure 2, it is noticed that the structure was changed from fine ($TaO_{0.2}N_{0.8}$) to rough, then, to fine feature again. Apparently, the hardness drop should be related to the amount of Ag. As far as the porosity is concerned, no evidence is found in this study that porosity is playing a critical role in these sputtered coating deposited with bias voltage. Although a previous study, has proved that the oxynitride coatings were dense and without porosity [19], one definitely cannot rule out the possibility of porosity effect. The highest hardness of these coatings can reach 27 GPa. Figure 4b shows the ratio of hardness to modulus (H/E) vs. Ag contents in the coatings. The H/E ratio is known to be treated as the index for the elastic strain to coating failure, which may be used as an index for cracking resistance [24]. This index could be critical when surgical implant is under sudden impact. Comparing with the properties of the as-deposited coatings, it is found that, after annealing, the H/E ratio tends to increase due to the emergence of soft Ag particles and toughening mechanisms [25], particularly for the coatings with 1.5 at. % Ag. It is worth noticing that the TaON sample without Ag doping had higher H/E value than that of TaN. This could be attributed to the substitution of Ta-N bonds with Ta-O bonds. At the same time, the original TaN cubic structure was maintained, as so was the fine structure (smaller column width). Both would withstand higher elastic strain before breaking.



(**a**) (**b**)

Figure 4. (**a**) Hardness and modulus vs. Ag contents, and (**b**) H/E vs. Ag contents.

3.3. Surface Morphology and Roughness

Figure 5 shows the AFM images of surface morphology for as-deposited and annealed samples. It is found the annealed samples tend to have higher roughness. Apparently, this is due to the emergence of Ag particles. Figure 6 shows the variation of roughness (Ra and Rmax) for as-deposited and annealed samples. The roughness increases after these samples were annealed. The increased roughness may be beneficial to cell attachment. However, it is also noticed that, when the Ag contents is at 11 at. %, the roughness is suddenly increased. Following the observation of the AFM image, it can be concluded that the large Ag particles contribute to the sudden increase of Ra and Rmax.

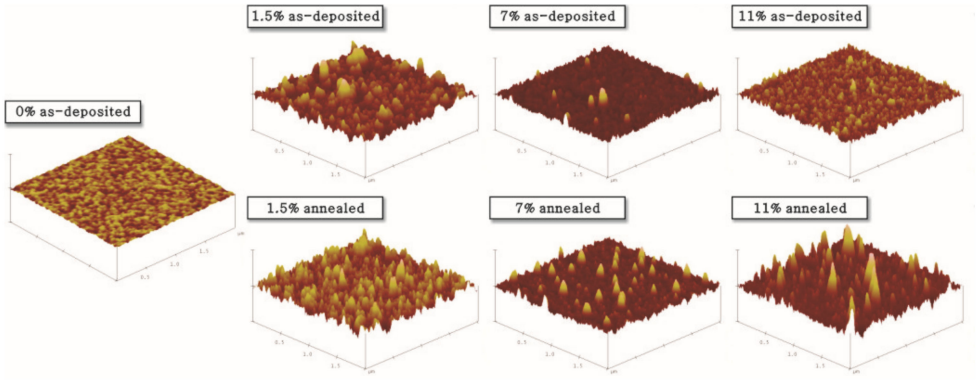


Figure 5. AFM images for $TaO_{0.2}N_{0.8}$ and $TaO_{0.2}N_{0.8}$-Ag coatings before and after annealing.

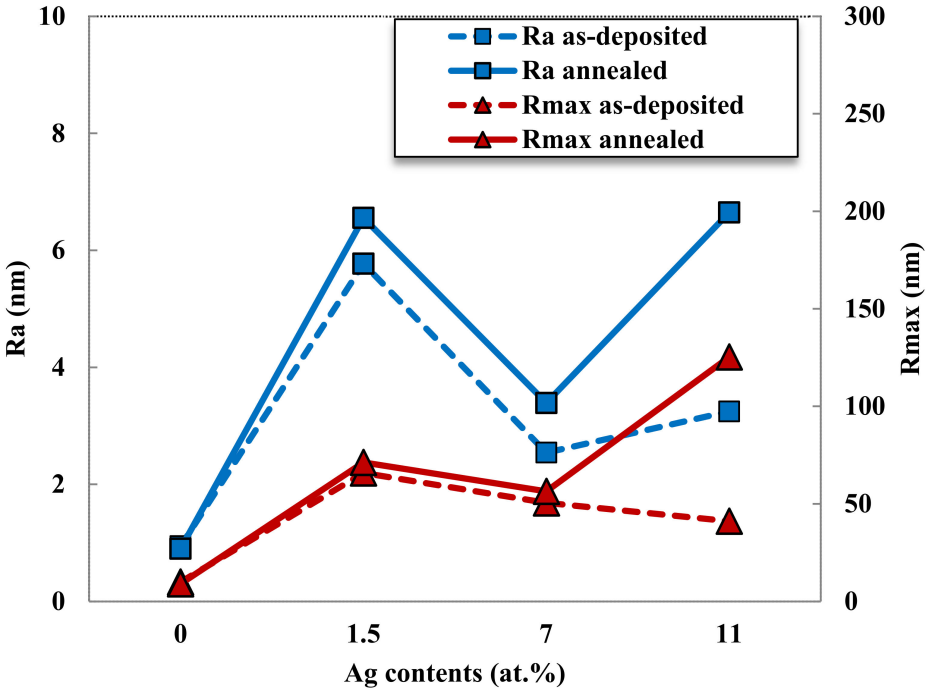


Figure 6. Surface roughness (Ra and Rmax) of $TaO_{0.2}N_{0.8}$ and $TaO_{0.2}N_{0.8}$-Ag coatings before and after annealing, as a function of Ag contents.

3.4. Biocompatibility

The bio-chemical-physical surface interactions occurs between inorganic biomaterials and living cells is known to be the controlling factors [26–28]. Therefore, it is reasonable to manipulate surface coatings in order to make the best in terms of biocompatibility. Generally speaking, these bio-properties can be classified to two critical interactions: (1) surface topography on the micro- and nano- meter scale. This factor would determine the cell adhesion and attachment [29,30], and (2) the surface energy. This factor would control electron transfer process as well as the electrical potential distribution. Both factors would surely affect biocompatibility [31].

It has been found that surface topography in the micro- and/or nano- meter scales can enhance protein and collagen production and cell attachment [29,30]. However, the effects of other bio-factors cannot be excluded as some cells can attach and differentiate on flat surfaces. This could be related to biochemistry. In addition to topography, surface energy may also affect bioactivity significantly. Surface with hydrophilic behavior, contrasting to hydrophobic normally shows improved cell attachment and proliferation [31,32]. In the present study, the effect of surface roughness on biocompatibility is the focused point, as the variation of Ag contents did not make coatings more, or less, hydrophilic.

In the biocompatibility testing part, 3T3 cells were selected and tested. The optical microscopy of the cultured 3T3 cells on the samples with and without rapid thermal annealing is shown in Figure 7 which presents the surface morphology after Day 1 and Day 7.

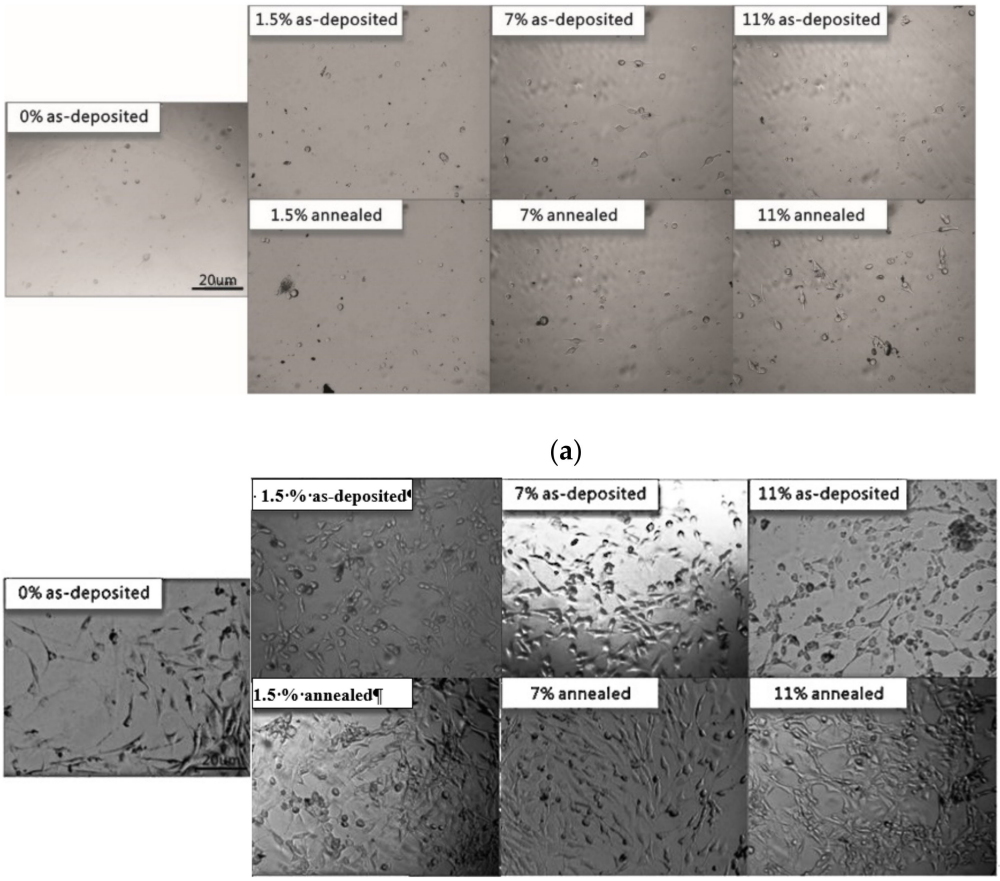


Figure 7. 3T3 fibroblast morphology cultured on $TaO_{0.2}N_{0.8}$ and $TaO_{0.2}N_{0.8}$-Ag coatings with and without annealing, as a function of Ag contents: (**a**) Day 1, and (**b**) Day 7, under optical microscope 200×.

From the variation in the shown images, it can be noticed that these cells tend to attach in an unregulated style. This is known to be the characteristic behavior of 3T3 cells. In the later stage, the attached cells normally would show typical 3T3 cell morphology. In this stage, an elongated and polygonal form should be observed. After the 3rd day through culturing period, beside well attached the 3T3 cells have shown migration and/or proliferation. Overall, it is observed that the cell density increases with Ag contents at 1.5 and 11 at. %. Apparently, this can be attributed to the increase of roughness partly due to the emergence of Ag particles.

MTT assay is normally applied to determine the amounts of mitochondria existing in viable cells. In the testing process, succinate dehydrogenase existing in mitochondria should react with tetrazolium. At the end, formazan (a purple crystal) should form. This chemical can be detected using a suitable optical approach. Mitochondria is known to be a type of energy harvest organelle inside the tested cells. The results can be used as a trustable index for checking the total cellular activities. The viable cell amounts can then be evaluated. This is carried out by checking the optical absorption intensity aiming at the wavelength around 570 nm. The mitochondria concentration will stand for the number of viable cells and, certainly, the biocompatibility. This is because that the amounts of mitochondria are proportional to the optical density. Hence, the MTT assay testing can be applied to evaluate the proliferation/apoptosis of cells through a certain time. Figure 8

shows the results obtained from the MTT assay tests. It can be seen from this figure that $TaO_{0.2}N_{0.8}$ coating exhibits little change from Day 1 to Day 7. The sample with 1.5 and 11 at. % Ag shows the highest optical density until Day 7. These two samples happen to have the highest value of roughness. In sum, the annealed samples show higher cell activity or viability. Comparing with Figure 6, it can be concluded that roughness is the major factor that control the cell attachment and proliferation. In addition, the emergence of Ag particles on the coating surface does not show any negative effect in terms of cell culturing.

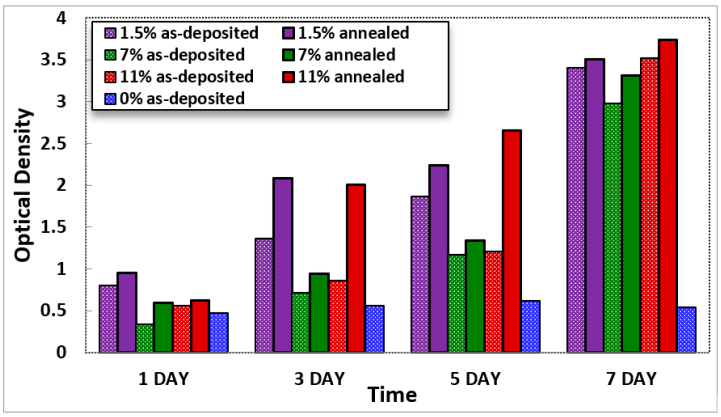


Figure 8. Viability of 3T3 cells cultured on $TaO_{0.2}N_{0.8}$ and $TaO_{0.2}N_{0.8}$-Ag coatings with and without annealing, as a function of Ag contents. The data are obtained using MTT assays.

3.5. Antibacterial Efficiency

The antibacterial efficiency as a function of Ag contents before and after annealing against E. coli is shown in Figure 9. According to these figures, the $TaO_{0.2}N_{0.8}$ and $TaO_{0.2}N_{0.8}$-Ag coatings, after being annealed, show that the antibacterial efficiency against E. coli is related to Ag contents and annealing condition, which may determine the exposed amount and particle size of Ag particles. Once dissolved, these particles would generate Ag ions which would then destroy the membrane or DNA of bacteria. The annealed coatings show good anti-bacterial behaviors against E. coli. As expected, the increased Ag contents, may increase the exposed Ag, and therefore the anti-bacterial efficiency. All the coatings show over 99% of antibacterial efficiency after immersion for 24 h, even the unannealed samples.

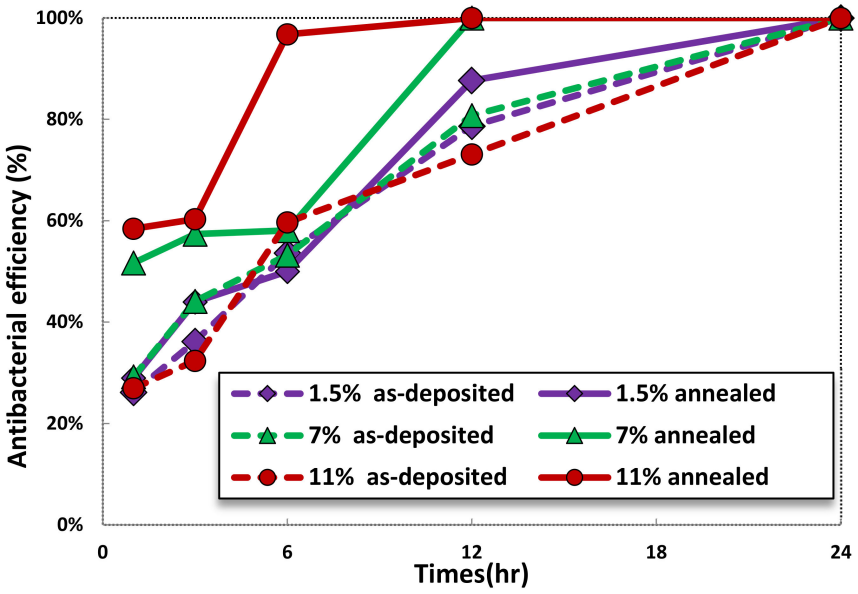


Figure 9. Antibacterial efficiency of $TaO_{0.2}N_{0.8}$ and $TaO_{0.2}N_{0.8}$-Ag coatings before and after annealing, as a function of Ag contents.

4. Conclusions

Unannealed and annealed $TaO_{0.2}N_{0.8}$ and $TaO_{0.2}N_{0.8}$-Ag coatings were prepared using reactive co-sputtering, followed by rapid thermal annealing in order to induce the emergence of Ag nanoparticles. The Ag-doped coatings have shown improved mechanical properties, particularly for the annealed sample with 1.5 at. % Ag. In addition, the surface morphology and emerged Ag particles is varied depending on the Ag contents and annealing conditions. This would affect the biocompatibility and antibacterial efficiency. The sample with 1.5 and 11 at. % Ag shows the highest surface roughness (Ra and Rmax). Consequently, they have the best biocompatibility with 3T3 cells. The increased Ag contents would increase the exposed Ag, and therefore the anti-bacterial efficiency. All the Ag-doped coatings show over 99% of antibacterial efficiency after immersion for 24 h, even the unannealed samples. Following the results of biocompatibility and MTT assay tests, one can conclude that surface roughness could be the dominating factor for cell attachment. No negative effect of the added Ag is found in this study. Accordingly, in the future, the studied coatings can be applied on surgical implant. However, the uniformity of coating on various implants with uneven shapes should be overcome. This would require many efforts from researchers, medical doctors, and engineers.

Author Contributions: Conceptualization, J.-H.H. and C.L.; methodology, J.-H.H., W.W., C.-C.H., Y.-H.C.; validation, J.-H.H. and C.L.; investigation, Y.-H.L. and S.-C.L.; writing—original draft preparation, J.-H.H.; writing—review and editing, C.L.; supervision, J.-H.H.; project administration, J.-H.H.; funding acquisition, J.-H.H. and C.-C.H. All authors have read and agreed to the published version of the manuscript.

Funding: This work was supported in part by the Ministry of Science and Technology, Taiwan under Grants MOST 103-2221-E-131-003-MY2 and MOST 108-2314-B-182A-077-MY3 are greatly appreciated.

Institutional Review Board Statement: Not applicable.

Informed Consent Statement: Not applicable.

Data Availability Statement: Not applicable.

Conflicts of Interest: The authors declare no conflict of interest.

References

1. Burdus, A.C.; Gherasim, O.; Andronescu, E.; Grumezescu, A.M.; Ficai, A. Inorganic nanoparticles in bone healing applications. *Pharmaceutics* **2022**, *14*, 770. [CrossRef] [PubMed]
2. Qing, Y.; Cheng, L.; Li, R.; Liu, G.; Zhang, Y.; Tang, X.; Wang, J.; Liu, H.; Qin, Y. Potential antibacterial mechanism of silver nanoparticles and the optimization of orthopedic implants by advanced modification technologies. *Int. J. Nanomed.* **2018**, *13*, 3311–3327. [CrossRef] [PubMed]
3. Poon, T.K.C.; Iyengar, K.P.; Jain, V.K. Silver Nanoparticle (AgNP) Technology ap-plications in trauma and orthopaedics. *J. Clin. Orthop. Trauma* **2021**, *21*, 101536. [CrossRef] [PubMed]
4. Kim, J.; Cho, M.; Oh, B.; Choi, S.; Yoon, J. Control of bacterial growth in water using synthesized inorganic disinfectant. *Chemosphere* **2004**, *55*, 775–780. [CrossRef] [PubMed]
5. Sondi, I.; Salopek-Sondi, B. Silver nanoparticles as antimicrobial agent: A case study on E-coli as a model for Gram-negative bacteria. *J. Col. Int. Sci.* **2004**, *275*, 177–182. [CrossRef]
6. Hsieh, J.H.; Liu, P.C.; Li, C.; Cheng, M.K.; Chang, S.Y. Mechanical properties of TaN-Cu nanocomposite thin coatings. *Surf. Coat. Technol.* **2008**, *202*, 5530–5534. [CrossRef]
7. Hsieh, J.H.; Yeh, T.H.; Li, C.; Chiu, C.H.; Huang, C.T. Antibacterial properties of TaN-(Ag, Cu) nanocomposite thin coatings. *Vacuum* **2013**, *87*, 160–163. [CrossRef]
8. Ratner, B.D.; Hoffman, A.S.; Schoen, F.J.; Lemons, J.E. *Biomaterials Science*, 2nd ed.; Elsevier Academic Press: Cambridge, MA, USA, 2004.
9. Laurila, T.; Zeng, K.; Kivilahti, J.K.; Molarius, J.; Riekkinen, T.; Suni, I. Tantalum carbide and nitride diffusion barriers for Cu metallisation. *Microelectron. Eng.* **2002**, *60*, 71–80.
10. Le Dréo, H.; Banakh, O.; Keppner, H.; Steinmann, H.A.; Briand, D.; de Rooij, N.F. Optical, electrical and mechanical properties of the tantalum oxynitride thin coatings deposited by pulsing reactive gas sputtering. *Thin Solid Films* **2006**, *515*, 952–956. [CrossRef]
11. Venkataraj, S.; Kittur, H.; Drese, R.; Wuttig, M. Multi-technique characterization of tantalum oxynitride coatings prepared by reactive direct current magnetron sputtering. *Thin Solid Films* **2006**, *514*, 1–9. [CrossRef]

12. Cristea, D.; Velicu, J.L.; Cunha, L.; Barradas, N.; Alves, E.; Craciun, V. Tantalum-Titanium Oxynitride Thin Coatings Deposited by DC Reactive Magnetron Co-Sputtering: Mechanical, Optical, and Electrical Characterization. *Coatings* **2022**, *12*, 36. [CrossRef]
13. Cristea, D.; Cunha, L.; Gabor, C.; Ghiuta, I.; Croitoru, C.; Marin, A.; Velicu, L.; Besleaga, A.; Vasile, B. Tantalum Oxynitride Thin Coatings: Assessment of the Photocatalytic Efficiency and Antimicrobial Capacity. *Nanomaterials* **2019**, *9*, 476. [CrossRef]
14. Tessier, F.; Marchand, R. Ternary and higher order rare-earth nitride materials: Synthesis and characterization of ionic-covalent oxynitride powders. *J. Solid State Chem.* **2003**, *171*, 143–151. [CrossRef]
15. Fuertes, A. Synthesis and properties of functional oxynitrides—From photocatalysts to CMR materials. *Dalton Trans.* **2010**, *39*, 5942–5948. [CrossRef]
16. Marchenko, E.; Baigonakova, G.; Kokorev, O.; Yasenchuk, Y.; Vorozhtsov, A. Biocompatibility Assessment of Coatings Obtained in Argon and Nitrogen Atmospheres for TiNi Materials. *Metals* **2022**, *12*, 1603. [CrossRef]
17. Banakh, O.; Steinmann, P.A.; Dumitrescu-Buforn, L. Optical and mechanical properties of tantalum oxynitride thin coatings deposited by reactive magnetron sputtering. *Thin Solid Films* **2006**, *513*, 136–141. [CrossRef]
18. Hsieh, J.H.; Chang, C.C.; Li, C.; Liu, S.J.; Chang, Y.K. Effects of Ag contents on antibacterial behaviors of TaON-Ag nanocomposite thin coatings. *Surf. Coat. Technol.* **2010**, *205*, S337–S340. [CrossRef]
19. Hsieh, J.H.; Lai, Y.H.; Lin, Y.C.; Liao, S.J.; Li, C.; Chang, Y.H.; Hu, C.C. Structure analysis, mechanical property, and biocompatibility of TaOxNy thin coatings. *Surf. Coat. Technol.* **2016**, *303*, 54–60. [CrossRef]
20. Hsieh, J.H.; Chiu, C.H.; Li, C.; Wu, W.; Chang, S.Y. Development of anti-wear and anti-bacteria TaN-(Ag, Cu) thin films—A review. *Surf. Coat. Technol.* **2013**, *233*, 159–168. [CrossRef]
21. Oliver, W.C.; Pharr, G.M. An improved technique for determining hardness and elastic modulus using load and displacement sensing indentation experiments. *J. Mater. Res.* **1992**, *7*, 1564–1583. [CrossRef]
22. Chen, J.; Bull, S.J. On the factors affecting the critical indenter penetration for measurement of coating hardness. *Vacuum* **2009**, *83*, 911–920. [CrossRef]
23. Hara, M.; Hitoki, G.; Takata, T.; Kondo, J.N.; Kobayashi, H.; Domen, K. TaON and Ta_3N_5 as new visible light driven photocatalysts. *Catal. Today* **2003**, *78*, 555–560. [CrossRef]
24. Leyland, A.; Mathew, A. On the significance of H/E ratio in wear control: A nanocomposite coating approach to optimized tribological behavior. *Wear* **2000**, *246*, 1–11. [CrossRef]
25. Musil, J.; Vlcek, J. Magnetron sputtering of hard nanocomposite coatings and their properties. *Surf. Coat. Technol.* **2001**, *142*, 557–566. [CrossRef]
26. Anderson, D.G.; Putnam, D.; Lavik, E.B.; Mahmood, T.A.; Langer, R. Biomaterial microarrays: Rapid, microscale screening of polymer-cell interaction. *Biomaterials* **2005**, *26*, 4892–4897. [CrossRef]
27. Hubbell, J.A. Biomaterials in tissue engineering. *Biotechnology* **1995**, *13*, 565–576. [CrossRef]
28. Fialho, L.; Alves, C.F.A.; Carvalho, F. A Decade of Progress on MAO-Treated Tantalum Surfaces: Advances and Contributions for Biomedical Appli-cations. *Nanomaterials* **2022**, *12*, 2319. [CrossRef]
29. Curtis, A.S.; Wilkinson, C.D. Reactions of cells to topography. *J. Biomater. Sci. Polym.* **1998**, *9*, 1313–1329. [CrossRef]
30. Wojciak-Stothard, B.; Curtis, A.; Monaghan, W.; MacDonald, K.; Wilkinson, C. Guidance and activation of murine macrophages by nanometric scale topography. *Exp. Cell Res.* **1996**, *223*, 426–435. [CrossRef]
31. Elwing, H.; Nilsson, B.; Svensson, K.E.; Askendahl, A.; Nilsson, U.R.; Lundstrom, I. Conformational changes of a model protein (complement factor-III) adsorbed on hydrophilic and hydrophobic solid surfaces. *J. Colloid Interface Sci.* **1988**, *125*, 139–145. [CrossRef]
32. van Wachem, P.B.; Beugeling, T.; Feijen, J.; Bantjes, A.; Detmers, J.P.; van Aken, W.G. Interaction of cultured human endothelial cells with polymeric surfaces of different wettability. *Biomaterials* **1985**, *6*, 403–408. [CrossRef]

Disclaimer/Publisher's Note: The statements, opinions and data contained in all publications are solely those of the individual author(s) and contributor(s) and not of MDPI and/or the editor(s). MDPI and/or the editor(s) disclaim responsibility for any injury to people or property resulting from any ideas, methods, instructions or products referred to in the content.